Terahertz Driven Amplification of Coherent Optical Phonons in GaAs Coupled to a Metasurface

Michael Woerner, Carmine Somma, Klaus Reimann, Thomas Elsaesser, Peter Q. Liu, Yuanmu Yang, John L. Reno, and Igal Brener

Phys. Rev. Lett. **122**, 107402 — Published 15 March 2019

DOI: 10.1103/PhysRevLett.122.107402

Terahertz driven amplification of coherent optical phonons in GaAs coupled to a metasurface

Michael Woerner,[1,*] Carmine Somma,[1] Klaus Reimann,[1] Thomas Elsaesser,[1]
Peter Q. Liu,[2,3] Yuanmu Yang,[2] John L. Reno,[2] and Igal Brener[2]

[1]*Max-Born-Institut für Nichtlineare Optik und Kurzzeitspektroskopie, 12489 Berlin, Germany*
[2]*Center for Integrated Nanotechnologies, Sandia National Laboratories, Albuquerque, New Mexico 87185, USA*
[3]*Department of Electrical Engineering, The State University of New York at Buffalo, Buffalo, New York 14260, USA*

(Dated: January 23, 2019)

We demonstrate amplification of longitudinal optical (LO) phonons by polar-optical interaction with an electron plasma in a GaAs structure coupled to a metallic metasurface using two-color two-dimensional spectroscopy. In a novel scheme, the metamaterial resonator enhances broadband terahertz fields, which generate coherent LO phonons and drive free electrons in the conduction band of GaAs. The time evolution of the LO phonon amplitude is monitored with mid-infrared pulses via the LO-phonon-induced Kerr nonlinearity of the sample, showing an amplification of the LO phonon amplitude by up to a factor of 10, in agreement with a theoretical estimate.

Amplification of sound in crystalline materials is a hot topic of current condensed-matter research, which provides new insight into coupled carrier-phonon dynamics and has resulted in novel ultrasound sources with high emission intensities at sub-THz frequencies. An interesting application of such ultrasound sources is in imaging, since spatial resolutions in the nm-range can be reached without ionizing radiation. Beginning with early work on the acousto-electric effect at frequencies of a few gigahertz [1–3], the amplification of acoustic phonons by interaction with electric currents has been studied in a variety of bulk semiconductors and, most recently, in semiconductor quantum wells and superlattices [4–8]. In the latter case, zone-folded acoustic phonons at frequencies of hundreds of gigahertz have been amplified by interaction with a tunneling or an intra-miniband current. Gain coefficients of up to $g = 10000\,\mathrm{cm}^{-1}$ have been observed [7].

Phonon amplification exploits the coupling of phonons and electrons via mechanisms like deformation potential, piezoelectric, or polar-optical interaction. The basic process for phonon amplification consists in the stimulated emission of phonons via intraband transitions of electrons. To amplify phonons with a wave vector $\mathbf{q}$ and an energy $\hbar\omega_{\mathbf{q}}$, the net gain has to compensate for phonon absorption and for spontaneous phonon decay into other lattice modes. This requires a population inversion within the carrier distribution $f_e(\mathbf{k})$, i.e., $\sum_{\mathbf{k}} [f_e(\mathbf{k}) - f_e(\mathbf{k}-\mathbf{q})]\, \delta [E(\mathbf{k}) - E(\mathbf{k}-\mathbf{q}) - \hbar\omega_{\mathbf{q}}] > 0$ with $E(\mathbf{k})$ the electron energy at $\mathbf{k}$. The preceding condition is valid for both acoustic and optical phonons, although the coupling mechanisms may be different. For acoustic phonon amplification one reaches population inversion once the drift velocity of the electron ensemble becomes larger than the sound velocity [7, 9]. In the experiments [6, 7], coherent acoustic phonons have been generated by femtosecond lasers and their amplification has been detected via time-resolved reflectivity measurements.

Figures 1(a) and (b) illustrate the inversion condition for optical phonons. A symmetric electron distribution centered at the Γ point [blue line in Fig. 1(a)] shows only phonon absorption, the inversion condition is met for no $\mathbf{q}$. In contrast, a *displaced* electron distribution [red line in Fig. 1(b)] shows phonon gain for a certain range of $\mathbf{q}$, determined by the electron displacement. For a small electron displacement the inversion condition is only met for phonons with large $\mathbf{q}$, phonons with smaller $\mathbf{q}$ reach the gain condition for larger electron displacements. To achieve a significant phonon gain, the electron displacement should be of the order of $q_0 = 2.5 \times 10^8\ \mathrm{m}^{-1}$ with $\hbar^2 q_0^2/2m_e = h\nu_{\mathrm{LO}}$, i.e., the wavevector where the electron has a kinetic energy equal to the phonon energy.

Amplification of optical phonons is much more difficult than that of acoustic phonons because of their different physical properties. First, optical phonons have a significantly higher energy than acoustic phonons, e.g., $\nu_{LO} = 9$ THz and $\nu_{TO} = 8$ THz for longitudinal (LO) and transverse (TO) optical phonons in GaAs [10]. Second, the inversion condition outlined above cannot be met under quasi-stationary conditions because of the huge heat load generated by a current sufficient for a stationary displacement of the electron distribution in k space of the order of q_0. Such issues call for new strategies to amplify optical phonons.

In this Letter, we use a combination of a metasurface with a GaAs heterostructure [11] and 2D spectroscopy [12] to demonstrate LO phonon amplification by a terahertz-driven *transient* electron distribution displaying inversion for optical phonons. Exploiting the partly longitudinal character of an enhanced THz field at the interface between a metallic resonator and a GaAs structure, a broadband THz pulse generates an initial LO phonon population and drives a Γ valley electron distribution to generate a transient population inversion for LO phonon amplification. The LO phonon amplitude is determined as a function of delay by the MIR probe pulse.

The sample studied here [Fig. 1(c)] consists of a 3-nm thick GaAs cap layer and a 40-nm thick AlAs layer grown on a 300-μm thick GaAs layer. The AlAs was added to avoid quenching of the optical phonon polarizability very close to the metal [13] and to prevent the exchange of electrons between the metal and the thick GaAs layer. The sample surface is covered with a metasurface consisting of a periodic square array (period 5 μm) of metallic dogbone resonators (MDRs) (see Fig. 1(d) and [14]). In our spectroscopic experiments with a

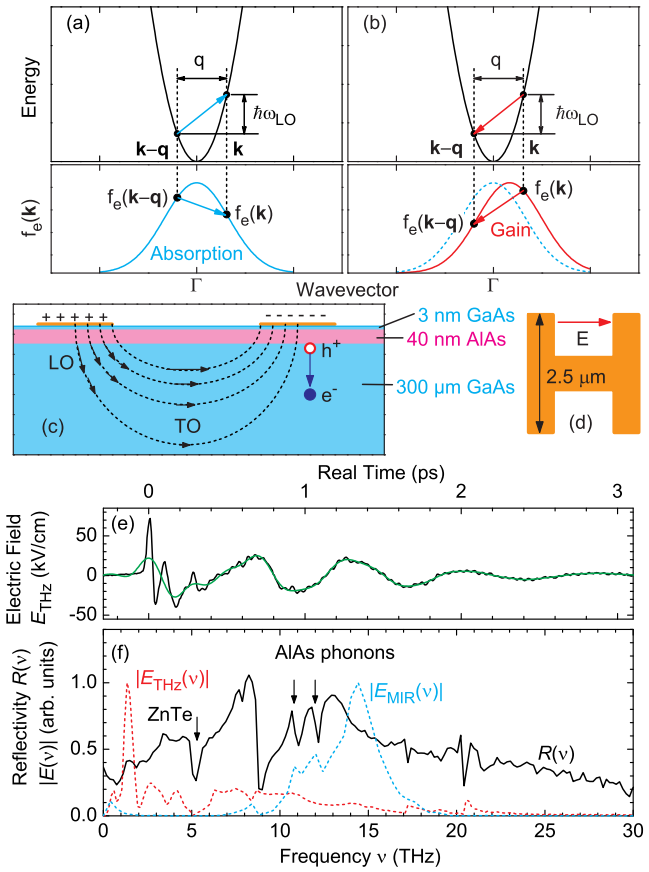

FIG. 1. (a), (b) The upper parts show the electron energy in the conduction band as a function of wavevector, the lower parts electron distribution functions. A phonon is absorbed when an electron is scattered from $\mathbf{k}-\mathbf{q}$ to $\mathbf{k}$ (the electron energy increases by $\hbar\omega_{\mathrm{LO}}$), a phonon is emitted when an electron is scattered from $\mathbf{k}$ to $\mathbf{k}-\mathbf{q}$ (the electron energy decreases by $\hbar\omega_{\mathrm{LO}}$). (a) Phonon absorption is more probable for $f_e(\mathbf{k}-\mathbf{q}) > f_e(\mathbf{k})$, (b) phonon emission (gain) for $f_e(\mathbf{k}-\mathbf{q}) < f_e(\mathbf{k})$. (c) Sample structure with the electric field distribution in the semiconductor layers underneath the MDRs. Right: strong electric fields create electron-hole pairs in GaAs. These electrons are accelerated into the thick GaAs layer thereby creating inversion for stimulated emission of coherent LO phonons. (d) Shape of the MDRs. (e) Black line: incident THz pump pulse $E^{\mathrm{in}}_{\mathrm{THz}}(t,\tau=0)$. The green curve shows a low-pass-filtered THz pump pulse without frequencies above 5 THz. (f) Spectrum of the THz pump pulse (red line) and of the MIR probe pulse (blue line). Black line: measured sample reflectivity $R(\nu) = |E_{\mathrm{re}}(\nu)/E_{\mathrm{in}}(\nu)|^2$.

spot diameter on the sample of some 100 μm, pulses in a frequency range from 1 to 20 THz interact with both the MDRs and the underlying semiconductor heterostructure. The metasurface was designed with its lowest resonance at 13 THz, corresponding to AlAs LO phonons, but off resonance to GaAs LO phonons [15]. Because the resonance is detuned significantly from the GaAs phonon frequency, the resonators do not provide an efficient radiative coupling pathway of LO phonons to free space, thus preventing a significant reduction of their lifetime. A numerical analysis of the electric field distribution underneath the MDRs reveals a roughly 15-fold and 5-fold enhancement of the incident transverse fields around 15 THz and 2 THz, respectively [14]. The enhanced field displays pronounced longitudinal components under the metallic resonators [arrows marked LO in Fig. 1(c)] extending down to the interface between AlAs and the thick GaAs layer, thus enabling an excitation of GaAs LO phonons at 9 THz [16–18].

In the 2D THz experiments, p-polarized broadband THz and mid-infrared (MIR) pulses are sent onto the sample under an angle of incidence of 20° [14]. The beams reflected from the sample are detected in amplitude and phase by free-space electrooptic sampling [19, 20] in ZnTe. Figure 1(e) shows the THz transient and Fig. 1(f) the spectra of both pulses. The THz spectrum extends from 1 to 15 THz, the MIR spectrum from 10 to 17 THz with a maximum at 15 THz.

The sample reflectivity $R(\nu) = |E_{\mathrm{re}}(\nu)/E_{\mathrm{in}}(\nu)|^2$ measured with the attenuated THz pulse is shown in Fig. 1(f). Here $E_{\mathrm{re}}(\nu)$ is the field reflected from the sample and $E_{\mathrm{in}}(\nu)$ is the field reflected from an unstructured gold layer. In the reststrahlen band of GaAs (8 to 9 THz), the reflectivity reaches almost unity. The strong field enhancement of the MDRs in the spectral range from 10 to 15 THz makes features corresponding to the optical phonons of the thin AlAs layer visible [21]. The dip at 5 THz is caused by the reststrahlen band of the electrooptic ZnTe crystal, the features at 17 and 20 THz by the minima of $|E_{\mathrm{THz}}(\nu)|$ (red line).

Results of the two-color 2D experiments are presented in Fig. 2. In the 2D scans we apply, in a collinear reflection geometry [14], both the THz pump pulse $E_{\mathrm{THz}}(t,\tau)$ [panel (a)] and the MIR probe pulse $E_{\mathrm{MIR}}(t)$ [panel (b)] to the sample and measure the nonlinearly emitted electric field $E_{\mathrm{NL}}(t,\tau) = E_{\mathrm{both}}(t,\tau) - E_{\mathrm{THz}}(t,\tau) - E_{\mathrm{MIR}}(t)$ [panel (c)] as a function of real time t and delay time τ [$E_{\mathrm{both}}(t,\tau)$: field with both pulses present]. Figure 2(d) shows the amplitude of the 2D Fourier transform $|\hat{E}_{\mathrm{NL}}(\nu_t,\nu_\tau)|$ of the nonlinear signal of panel (c). One sees signals for ν_t in the range of $E_{\mathrm{MIR}}(\nu)$, whereas there are signals at $\nu_\tau = 0$, ± 9, and ± 18 THz. The nonlinearly emitted MIR field $E_{\mathrm{NL}}(t,\tau = 437\ \mathrm{fs})$ [red line in Fig. 2(e)] is a 90° phase-shifted replica of the MIR pulse and displays an amplitude of more than 10 kV/cm. As a function of delay time τ, this behavior is repeated periodically with the LO phonon period, as illustrated by the cut $E_{NL}(0,\tau)$ in Fig. 3(c) (black solid line).

In a reference experiment [14], we applied a THz pulse without the 9-THz frequency component. Under such conditions, there is no nonlinear response at all. We conclude that excitation of the thick GaAs layer by the 9-THz component, i.e., at the LO phonon frequency, is essential for generating the pronounced nonlinear response shown in Fig. 2(c). Interestingly, pure phonon nonlinearities of the GaAs optical phonons, which would show up in Fig. 2(d) at $\nu_t = 9$ THz, are not observed. An estimate shows that an (internal) electric field of 1 MV/cm corresponds to a nonequilibrium phonon population of only 2×10^{-4}, way too low to observe pure phonon nonlinearities.

The experimental results can be explained by nonlinear

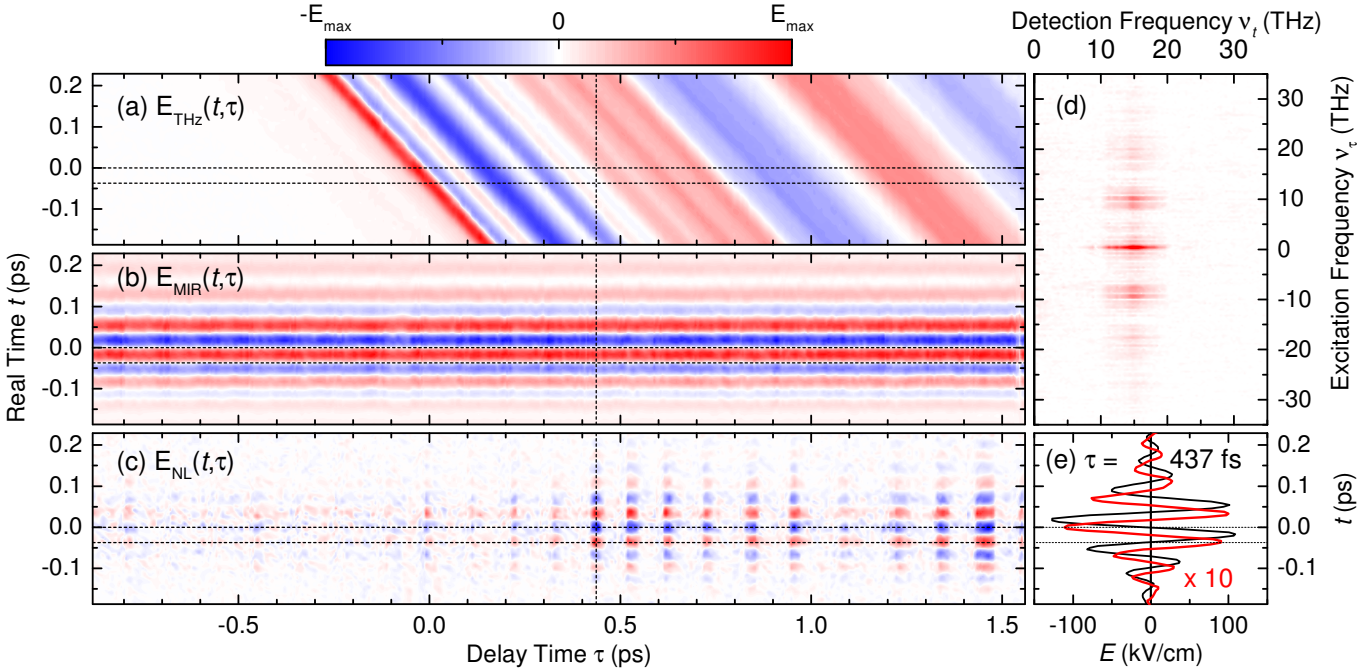

FIG. 2. Two-dimensional nonlinear terahertz spectroscopy performed on our sample. Measured reflected electric fields as a function of real time t and delay time τ: (a) the THz pump pulse $E_{\mathrm{THz}}(t,\tau)$, (b) the MIR probe pulse $E_{\mathrm{MIR}}(t,\tau)$, and (c) the nonlinearly emitted electric field $E_{\mathrm{NL}}(t,\tau)$. The values for $E_{\max}$ are: (a) 33, (b) 150, and (c) 12 kV/cm. (d) Amplitude of the 2D Fourier transform $|\hat{E}_{\mathrm{NL}}(\nu_t,\nu_\tau)|$ of the nonlinear signal. (e) Red curve: $E_{\mathrm{NL}}(t,\tau=437\ \mathrm{fs})$ [vertical dashed line in (a) to (c)] compared to the probe pulse $E_{\mathrm{MIR}}(t,\tau=437\ \mathrm{fs})$ (black line). The horizontal dashed lines in (a) to (c) and (e) illustrate the 90° phase shift between $E_{\mathrm{NL}}(t,\tau)$ and $E_{\mathrm{MIR}}(t,\tau)$.

light-matter interaction involving longitudinal phonon amplification. In this picture the 9 THz component generates coherent LO phonons, which are amplified by interaction with a current driven by the 1.5 THz component. The longitudinal 9 THz field component generated by the MDRs extends into the thick GaAs layer [Fig. 1(c)] and generates a coherent LO phonon excitation via the infrared transition dipole. The field enhancement in the thick GaAs layer by the MDRs results in 1.5 THz electric field strengths larger than 100 kV/cm. Such fields generate a coherent superposition of valence and conduction band eigenstates and move the coupled wavefunctions or 'virtual' carriers over a wide range in k-space [22]. Decoherence destroys the coherent superposition (the virtual carriers become real) within a very short time, effectively leading to a promotion of electrons from the valence band into the Γ minimum of the conduction band [23, 24]. Such electrons gain energy by interaction with the THz field, in particular in the extended subpicosecond periods over which the sub-5 THz frequency components of the broadband pulses exist [Fig. 1(e)]. The corresponding vector potential $A(t,\tau=0) = A(0,t) = \int_{-\infty}^{t} ds\, E_{\mathrm{THz}}(s,\tau=0)$ is shown in Fig. 3(a) [25]. For a cycle-averaged motion with electron energies well above the threshold of phonon emission the corresponding electron distribution in the Γ valley shows at most instants of time an inversion situation, allowing for the stimulated emission of LO phonons. The electric field leads to a movement of the electrons generated into the material, whereas the generated hole distribution is clamped at the AlAs/GaAs interface. Together, this results in an electric field E_{SC} pointing away from the AlAs/GaAs interface.

Interaction of coherent LO phonons with this inverted electron distribution via the polar-optical coupling results in stimulated LO phonon emission, i.e., amplification of the initial LO phonon excitation induced by the THz pulse. The connected longitudinal LO phonon polarization is enhanced concomitantly. The LO phonon amplification mechanism is illustrated in Fig. 1(b). Electrons promoted to the conduction band [23, 24] are displaced in k-space (red distribution function) by the large vector potential $A(t)$ of the THz pulse [22]. The coherent phonons kicked off by the initial part of the pump pulse [Fig. 3(a)] thus experience amplification during periods of large amplitudes of $A(t)$.

We now address the readout of LO phonon amplification with the MIR pulse. This pulse is nonresonant to the optical phonons between 8 and 9 THz and to the bandgap of GaAs around 400 THz. The emitted MIR field shown in Fig. 2(e) displays a 90° phase-shift relative to the incoming MIR pulse. A 90° phase-shift of $E_{\mathrm{NL}}(t=0,\tau)$ to earlier times corresponds to a refractive index change of $\Delta n/n \approx -2\%$ [26–29]. This index change is caused by the THz-generated electron-hole plasma via a 'Drude-like' contribution and, more importantly, by the internal electric field $E_{\mathrm{LO}}(t,\tau)$ originating from the LO phonon, which involves relative movements of anions and cations. Being longitudinal, $E_{\mathrm{LO}}(t,\tau)$ does not di-

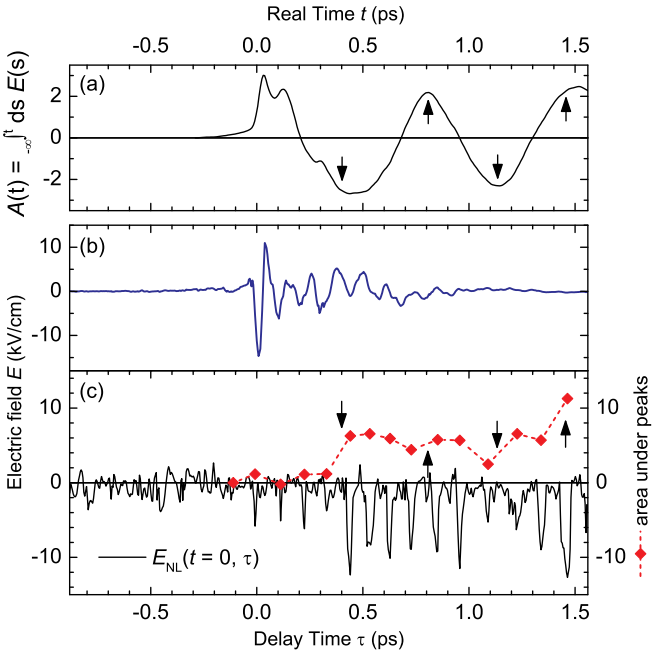

FIG. 3. (a) Time-dependent vector potential of the broadband THz pulses obtained from $E_{\mathrm{THz}}(t,\tau=0)$ in Fig. 2(a) [25]. The arrows indicate times for which the areas under the peaks [diamonds in panel (c)] show the steepest climbs. (b) (Linearly) emitted electric field by the GaAs TO phonons in the sample gained by a subtraction of the incident from the reflected THz field $E_{\mathrm{TO}}(\tau)=E^{\mathrm{re}}_{\mathrm{THz}}(t=0,\tau)-E^{\mathrm{in}}_{\mathrm{THz}}(t=0,\tau)$. (c) Nonlinearly emitted electric field $E_{\mathrm{NL}}(t=0,\tau)$ (black line) [horizontal dashed line at $t=0$ in Fig. 2(c)]. The area under the individual peaks (diamonds) is proportional to the coherent LO phonon population.

rectly contribute to the reflection, but it changes the refractive index for the MIR pulse via the Kerr effect. Since E_{THz} and E_{SC} also contribute to the Kerr effect, the MIR pulse experiences a quasi-instantaneous Kerr nonlinearity $\Delta n(t,\tau)\propto[E_{\mathrm{LO}}(t,\tau)+E_{\mathrm{THz}}(t,\tau)+E_{\mathrm{SC}}(t,\tau)]^2$, resulting in a nonlinear signal $E_{\mathrm{NL}}(t,\tau)$ proportional to $\Delta n(t,\tau)$. Because of the quadratic field dependence, the resulting nonlinear signal has Fourier components at $\nu_\tau=0$, $\pm\nu_{\mathrm{LO}}$, and $\pm2\nu_{\mathrm{LO}}$ [Fig. 2(d)]. The predominance of the LO phonon contribution is evident from the absence of a nonlinear signal in the reference experiment where electrons are driven by the THz pulse without initially exciting coherent phonons.

Most important is the fact that $E_{\mathrm{NL}}(t,\tau)$ plotted as the black line in Fig. 3(c) consists of a series of peaks separated by the LO phonon oscillation period $(\nu_{\mathrm{LO}})^{-1}$= (9 THz)$^{-1}$=115 fs. The area under the individual peaks, a measure for the coherent LO phonon amplitude, displays a substantial increase with τ [red diamonds in panel (c)], well beyond the duration of the 9 THz component of the broadband THz pulse [Fig. 1(e)]. This rise is a hallmark of amplification of the initially excited LO phonons. The times at which pronounced increases of the LO phonon amplitude occur are marked by arrows in Fig. 3(c) and agree well with the minima or maxima of the vector potential of the THz pulse [Fig. 3(a)]. At these times, the displacement of the electron distribution in k-space is highest [Fig. 1(b)], leading to the highest gain.

While the THz signal reflected from the sample contains emission from TO phonons, emission from LO phonons is absent as expected for a longitudinal polarization. The TO phonon signal shown in Fig. 3(b) decreases with delay time since TO phonons interact only weakly with Γ valley electrons and therefore do not experience gain.

Taking an electron distribution generated in the region of k-space with high interband transition dipoles [23] we calculated the time-dependent gain coefficient for LO phonon amplification determined by the large THz vector potential $A(t,\tau)$ of the THz pulse. Details of the theoretical model are given in [14]. The calculations give an amplification factor of 5 to 10, in good agreement with the experimental results in Fig. 3(c). The theoretical analysis predicts a delayed onset of amplification due to the buildup of the electron population inversion from carrier cooling. Moreover, there are periods of phonon reabsorption whenever the electron distribution driven by $A(t,\tau)$ passes the range of small k-vectors [cf. Fig. 1(a)]. Such mechanisms are behind the delayed step-like increase of the LO phonon amplitude shown in Fig. 3(c).

In conclusion, two-dimensional two-color THz spectroscopy on a nano-layered semiconductor structure covered by a metasurface made of metallic MDRs reveals clear signatures of coherent optical phonon amplification. In the experiments, we apply THz fields enhanced and modified by the MDRs to generate coherent LO phonons and an electron distribution in the conduction band of GaAs. Electrons periodically accelerated in the THz field allow for amplification of coherent LO phonons within a 1.5 ps time range. Amplification is due to stimulated phonon emission by the THz-driven electrons. This novel amplification scheme holds potential for a range of applications in phononics [30–33]. Since optical phonons are nonpropagating because of their weak dispersion, they can not be directly used for imaging. However, one can generate optical phonons in one material and use these to generate acoustic phonons with the same frequency in another material, potentially allowing sub-nanometer spatial resolution. Obviously, sources of optical phonons can also be used for the study of optical phonons themselves, which are important for many material properties like transport and superconductivity.

We acknowledge financial support by the Deutsche Forschungsgemeinschaft: RE 806/9-1. IB and PQL acknowledge support of the U.S. Department of Energy (DOE), Office of Basic Energy Sciences (BES), Division of Materials Sciences and Engineering. This work is performed in part at the Center for Integrated Nanotechnologies (the Sandia National Laboratories site), an U.S. DOE Office of Science User Facility operated jointly by the Sandia National Laboratories and the Los Alamos National Laboratories. Sandia National Laboratories is a multi-mission laboratory managed and operated by National Technology and Engineering Solutions of Sandia, LLC., a wholly owned subsidiary of Honeywell International,

Inc., for the U.S. Department of Energy's National Nuclear Security Administration under contract DE-NA0003525. The views expressed in the article do not necessarily represent the views of the U.S. Department of Energy or the United States Government.

* woerner@mbi-berlin.de

[1] R. H. Parmenter, The Acousto-Electric Effect, Phys. Rev. **89**, 990 (1953).

[2] G. Weinreich and H. G. White, Observation of the Acoustoelectric Effect, Phys. Rev. **106**, 1104 (1957).

[3] A. R. Hutson, J. H. McFee, and D. L. White, Ultrasonic Amplification in CdS, Phys. Rev. Lett. **7**, 237 (1961).

[4] S. M. Komirenko, K. W. Kim, A. A. Demidenko, V. A. Kochelap, and M. A. Stroscio, Generation and amplification of sub-THz coherent acoustic phonons under the drift of two-dimensional electrons, Phys. Rev. B **62**, 7459 (2000).

[5] A. J. Kent, R. N. Kini, N. M. Stanton, M. Henini, B. A. Glavin, V. A. Kochelap, and T. L. Linnik, Acoustic Phonon Emission from a Weakly Coupled Superlattice Under Vertical Electron Transport: Observation of Phonon Resonance, Phys. Rev. Lett. **96**, 215504 (2006).

[6] R. P. Beardsley, A. V. Akimov, M. Henini, and A. J. Kent, Coherent Terahertz Sound Amplification and Spectral Line Narrowing in a Stark Ladder Superlattice, Phys. Rev. Lett. **104**, 085501 (2010).

[7] K. Shinokita, K. Reimann, M. Woerner, T. Elsaesser, R. Hey, and C. Flytzanis, Strong Amplification of Coherent Acoustic Phonons by Intraminiband Currents in a Semiconductor Superlattice, Phys. Rev. Lett. **116**, 075504 (2016).

[8] A. V. Akimov, C. L. Poyser, and A. J. Kent, Review of microwave electro-phononics in semiconductor nanostructures, Semicond. Sci. Technol. **32**, 053003 (2017).

[9] S. Y. Mensah, F. K. A. Allotey, N. G. Mensah, and V. W. Elloh, Amplification of acoustic phonons in a degenerate semiconductor superlattice, Physica E **19**, 257 (2003).

[10] D. J. Lockwood, G. Yu, and N. L. Rowell, Optical phonon frequencies and damping in AlAs, GaP, GaAs, InP, InAs and InSb studied by oblique incidence infrared spectroscopy, Solid State Commun. **136**, 404 (2005).

[11] A. Benz, S. Campione, S. Liu, I. Montaño, J. F. Klem, A. Allerman, J. R. Wendt, M. B. Sinclair, F. Capolino, and I. Brener, Strong coupling in the sub-wavelength limit using metamaterial nanocavities, Nature Commun. **4**, 2882 (2013).

[12] M. Woerner, W. Kuehn, P. Bowlan, K. Reimann, and T. Elsaesser, Ultrafast two-dimensional terahertz spectroscopy of elementary excitations in solids, New J. Phys. **15**, 025039 (2013).

[13] P. Q. Liu, J. L. Reno, and I. Brener, Quenching of Infrared-Active Optical Phonons in Nanolayers of Crystalline Materials by Graphene Surface Plasmons, ACS Photonics **5**, 2706 (2018).

[14] See Supplemental Material at http://link.aps.org/supplemental/10.1103/PhysRevLett.xxx, which includes Refs. [34–38] and contains additional details on the sample design, the experimental setup, the inversion model, the results from an experiment without the initial 9-THz component, and nonlinear data in an extended t range.

[15] A. Benz, S. Campione, J. F. Klem, M. B. Sinclair, and I. Brener, Control of Strong Light–Matter Coupling Using the Capacitance of Metamaterial Nanocavities, Nano Lett. **15**, 1959 (2015).

[16] R. Ruppin, Surface effects on optical phonons and on phonon-plasmon modes, Surf. Sci. **34**, 20 (1973). Strictly speaking, the optical phonons considered in the nanolayered sample are interface phonon modes. Optical phonons polarized perpendicular to the layers have properties similar to bulk LO phonons, those with a parallel polarization have properties similar to bulk TO phonons.

[17] D. W. Berreman, Infrared Absorption at Longitudinal Optic Frequency in Cubic Crystal Films, Phys. Rev. **130**, 2193 (1963).

[18] C. Colvard, T. A. Gant, M. V. Klein, R. Merlin, R. Fischer, H. Morkoc, and A. C. Gossard, Folded acoustic and quantized optic phonons in (GaAl)As superlattices, Phys. Rev. B **31**, 2080 (1985).

[19] Q. Wu and X.-C. Zhang, Free-space electro-optics sampling of mid-infrared pulses, Appl. Phys. Lett. **71**, 1285 (1997).

[20] K. Reimann, R. P. Smith, A. M. Weiner, T. Elsaesser, and M. Woerner, Direct field-resolved detection of terahertz transients with amplitudes of megavolts per centimeter, Opt. Lett. **28**, 471 (2003).

[21] Although the MDRs resonantly enhance the linear response of AlAs optical phonons, any nonlinear response from AlAs phonons was not observed.

[22] W. Kuehn, P. Gaal, K. Reimann, M. Woerner, T. Elsaesser, and R. Hey, Coherent Ballistic Motion of Electrons in a Periodic Potential, Phys. Rev. Lett. **104**, 146602 (2010).

[23] W. Kuehn, P. Gaal, K. Reimann, M. Woerner, T. Elsaesser, and R. Hey, THz-induced interband tunneling of electrons in GaAs, Phys. Rev. B **82**, 075204 (2010).

[24] C. Lange, T. Maag, M. Hohenleutner, S. Baierl, O. Schubert, E. R. J. Edwards, D. Bougeard, G. Woltersdorf, and R. Huber, Extremely Nonperturbative Nonlinearities in GaAs Driven by Atomically Strong Terahertz Fields in Gold Metamaterials, Phys. Rev. Lett. **113**, 227401 (2014).

[25] The THz pulse $E_{\mathrm{THz}}(t,\tau)$ and consequently its vector potential $A_{\mathrm{THz}}(t,\tau)$ exhibit the symmetry $E_{\mathrm{THz}}(t,\tau) = E_{\mathrm{THz}}(\tau,t)$ in the 2-dimensional (t,τ) space. The same symmetry holds for the vector potential.

[26] J. J. Wynne and G. D. Boyd, Study of optical difference mixing in Ge and Si using a CO_2 gas laser, Appl. Phys. Lett. **12**, 191 (1968).

[27] S. S. Jha and N. Bloembergen, Nonlinear Optical Susceptibilities in Group-IV and III-V Semiconductors, Phys. Rev. **171**, 891 (1968).

[28] J. J. Wynne, Optical Third-Order Mixing in GaAs, Ge, Si, and InAs, Phys. Rev. **178**, 1295 (1969).

[29] W. K. Burns and N. Bloembergen, Third-Harmonic Generation in Absorbing Media of Cubic or Isotropic Symmetry, Phys. Rev. B **4**, 3437 (1971).

[30] M. Maldovan, Sound and heat revolutions in phononics, Nature **503**, 209 (2013).

[31] M. Aspelmeyer, T. J. Kippenberg, and F. Marquardt, Cavity optomechanics, Rev. Mod. Phys. **86**, 1391 (2014).

[32] J. B. Khurgin, Relative merits of phononics vs. plasmonics: the energy balance approach, Nanophotonics **7**, 305 (2018).

[33] A. von Hoegen, R. Mankowsky, M. Fechner, M. Först, and A. Cavalleri, Probing the interatomic potential of solids with strong-field nonlinear phononics, Nature **555**, 79 (2018).

[34] C. Somma, G. Folpini, J. Gupta, K. Reimann, M. Woerner, and T. Elsaesser, Ultra-broadband terahertz pulses generated in the organic crystal DSTMS, Opt. Lett. **40**, 3404 (2015).

[35] W. Kuehn, K. Reimann, M. Woerner, T. Elsaesser, and R. Hey, Two-Dimensional Terahertz Correlation Spectra of Electronic Excitations in Semiconductor Quantum Wells, J. Phys. Chem. B **115**, 5448 (2011).

[36] T. Kuhn, Density matrix theory of coherent ultrafast dynamics, in *Theory of Transport Properties of Semiconductor Nanostructures*, edited by E. Schöll (Chapman & Hall, London, 1998) pp. 173–214.

[37] J. Shah, *Ultrafast Spectroscopy of Semiconductors and Semiconductor Nanostructures*, 2nd ed. (Springer, Berlin, 1999).

[38] B. K. Ridley, Electron-phonon interaction in 2D systems, in *Hot Carriers in Semiconductor Nanostructures*, edited by J. Shah (Academic Press, Boston, 1992) pp. 17–51.